Dalton Transactions

ROYAL SOCIETY OF CHEMISTRY

PAPER

View Article Online
View Journal | View Issue

Cite this: *Dalton Trans.*, 2026, **55**, 2556

A change in ligand hapticity promotes Lewis base dissociation

Payton A. Fortuna,†[a] Leslie S. G. Kelley,†[a] Yipeng Sun,[b] Jiabin Xu,[a] Zhiqiang Wang,[a] Paul D. Boyle,[a] Tsun-Kong Sham,*[a] Viktor N. Staroverov*[a] and Johanna M. Blacquiere*[a]

Received 7th October 2025,
Accepted 12th January 2026

DOI: 10.1039/d5dt02402a

rsc.li/dalton

We report a phosphine 1-azaallyl ligand **L2** [2-(diphenylphosphino)-2′-(3,3-dimethyl-1-azaallyl)-1,1′-biphenyl], which enables reversible coordination of Lewis bases through changes in ligand hapticity. In the palladium methyl complex [Pd(CH$_3$)(**L2**)], **L2** adopts a κ^1-P;η^3-NCC coordination mode. Pyridine binding induces reorganization to a κ^2-PN mode, while reversion to the κ^1-P;η^3-NCC mode facilitates pyridine dissociation. These interconversions were established by $^{13}C\{^1H\}$ and $^1H-^{31}P$ HMBC NMR spectroscopy, X-ray absorption spectroscopy, and density-functional theory calculations. The results highlight a ligand-controlled mechanism for reversible substrate coordination based on tunable binding modes.

Introduction

Ligand substitution is a fundamental reaction step that is common among nearly all mechanisms of transition metal catalysis.[1,2] Catalyst turnover requires that product molecules generated at the metal centre be displaced by an incoming substrate (Fig. 1a). Mechanistically, this can occur through either associative or dissociative pathways.[3] In some cases, this step is rate-limiting, and strong product binding can inhibit catalytic activity. Consequently, ligand features that promote efficient product dissociation without compromising substrate binding are highly desirable in the catalyst design.

Several ligand characteristics are known to facilitate substitution reactions. For example, dissociation can be enhanced through electronic effects associated with strong *trans*-effect ligands or through steric congestion imposed by bulky ancillary ligands.[1,2] Hemilabile ligands have also been widely explored as a strategy to promote substitution chemistry, as low barrier isomerization between different coordination modes can reversibly open and close coordination sites at the metal centre.[4–7] Classical hemilabile ligands involve changes in denticity (*e.g.* $\kappa^2 \leftrightarrow \kappa^1$, $\kappa^3 \leftrightarrow \kappa^2$), but other strategies to alter metal coordination properties include changes in hapticity or switches in donor type arising from distinct ligand resonance forms.[4,8–11] A canonical example of the former is the indenyl ligand, which facilitates associative substitution reactions *via* ring slippage (*i.e.*, $\eta^5 \leftrightarrow \eta^3$; Fig. 1b).[12–14]

The 1-azaallyl ligand has a four-electron delocalized π-system, across an anionic NCC fragment, that engenders a variety of coordination modes, with one or two coordination sites at a metal.[15] Lappert demonstrated that Ni(II) and Pd(II) bis(1-azaallyl) complexes exhibit η^3-NCC ligand coordination, while chemical exchange of the ligand substituents was rationalized based on an isomerization *via* an η^1-N (*i.e.*, κ^1-N) coordination mode.[16] This change in hapticity means the ligand readily toggles between coordination to one and two sites on the metal. To take advantage of this versatile coordination chemistry, we have integrated the 1-azaallyl moiety into a ligand structure that also includes a monodentate phosphine donor (**L1**, Fig. 2).[17] The ligand readily binds to Ru(II) or Pd(II) metal fragments through a bidentate mode (*i.e.*, κ^2-PN; Fig. 2, *e.g.* Pd(II), **A**).[17,18] This mode was enforced through the metal coordination geometry and the presence of excess donor ligands (pyridine molecules). In the absence of donor ligands,

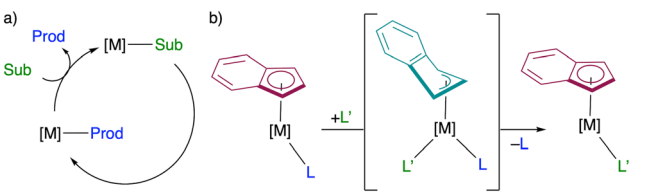

Fig. 1 Examples of ligand substitution reactions relevant to catalysis: (a) substitution of incoming substrate (sub) for product (prod) in catalytic intermediates, and (b) generic depiction of indenyl slippage, which permits associative substitution at coordinatively saturated metals. [M] represents a generic metal with undefined ancillary ligand coordination.

[a]*Department of Chemistry, The University of Western Ontario, London, N6A 3K7, Canada. E-mail: tsham@uwo.ca, vstarove@uwo.ca, johanna.blacquiere@uwo.ca*
[b]*Department of Mechanical and Materials Engineering, The University of Western Ontario, London, N6A 5B9, Canada*
† These authors contributed equally.

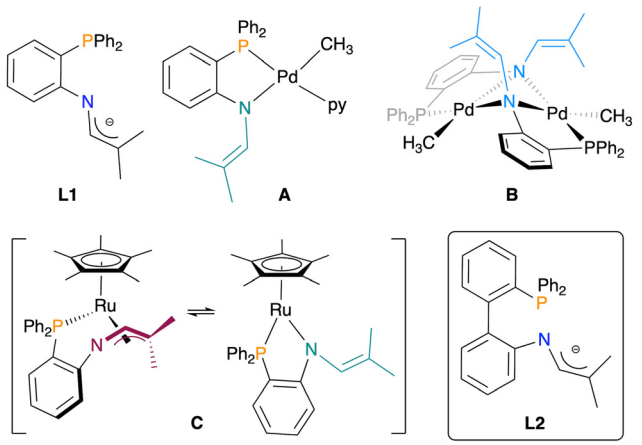

Fig. 2 Previously reported phosphine 1-azaallyl ligand **L1**, corresponding complexes **A**–**C**, and the new ligand **L2** reported herein.

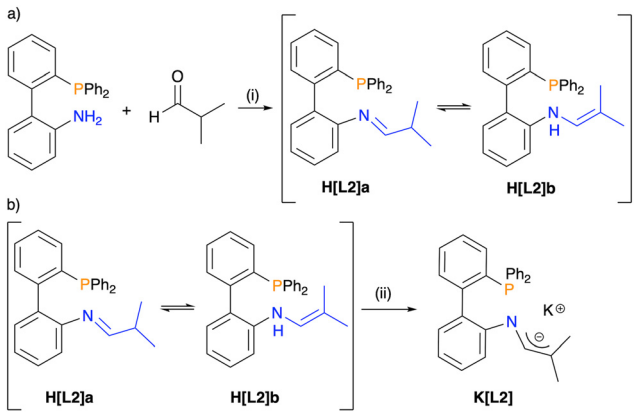

Scheme 1 Synthesis of (a) phosphine imine/enamine tautomers **H[L2]** and (b) deprotonated ligand salt **K[L2]**. Reaction conditions: (i) formic acid, toluene, 4 Å molecular sieves, rt, 24 h; (ii) 1 equiv. K[HMDS], THF, rt, 0.5 h.

the 1-azaallyl fragment stabilizes a Pd–Me moiety by μ-N bridging in complex **B**.[18] Ligation of **L1** to a Ru–Cp* fragment (Cp* = 1,2,3,4,5-pentamethylcyclopentadienyl) afforded **C**, which does not have a placeholder ligand, and the 1-azaallyl group exhibited rapid exchange ascribed to an η^3-NCC ↔ κ^1-N interconversion.[19] While the κ^1-P;η^3-NCC coordination mode of **L1** was supported by electronic structure calculations, it had not been observed spectroscopically. Presumably, the relatively small P–M–N bite angle is preferrable for κ^2-PN, rather than κ^1-P;η^3-NCC, coordination.

Herein, we report preparation of a new phosphine 1-azaallyl ligand (**L2**), which could more readily access a κ^1-P;η^3-NCC coordination mode. We targeted a Pd(II) complex, both since this metal is frequently used as a model system for substitution chemistry and because it has broad relevance in catalysis. The coordination chemistry of **L2** was evaluated through a range of spectroscopic and computational means. The impact of the coordination mode on substitution chemistry was probed, and experiments reveal ligand **L2** promotes Lewis base dissociation.

Results and discussion

Synthesis of ligands and complexes

A condensation reaction between 2′-(diphenylphosphanyl)-[1,1′-biphenyl]-2-amine and isobutyraldehyde was performed to afford **H[L2]**, as a white solid with an average yield of 87% (Scheme 1a). The $^{31}P\{^1H\}$ NMR spectrum of the isolated product in $CDCl_3$ has two distinct singlets at δ_P = −12.4 and −13.3 in a 1 : 2 ratio. The ^1H NMR spectrum also exhibits two sets of signals for product **H[L2]**. One set includes a doublet at δ_H = 7.55 consistent with an imine proton, as well as a doublet of septets at δ_H = 2.39 and a broad multiplet in the range of δ_H = 0.97–0.89 that were assigned to an *iso*-propyl group. These signals support the presence of the expected imine tautomer, **H[L2]a**. The second set of signals includes two singlets at δ_H = 1.69 and 1.36, assigned to two inequivalent methyl groups, and two doublets at δ_H = 6.08 and 4.94 correspond to vinyl and N–H protons, respectively. This pattern is consistent with the enamine tautomer, **H[L2]b**.

Deprotonation of **H[L2]** with K[HMDS] was performed to afford the phosphine 1-azaallyl ligand **K[L2]**, as an orange solid in a 76% yield (Scheme 1b). The $^{31}P\{^1H\}$ NMR spectrum of **K[L2]** has one singlet at δ_P = −13.6, confirming deprotonation of both tautomers to give one species. Successful deprotonation is further confirmed by the ^1H NMR spectrum of **K[L2]**, where the methine proton of **H[L2]a** and the N–H proton of **H[L2]b** are no longer observed.

The tautomeric mixture of the neutral ligand **H[L2]a**/**H[L2]b** was coordinated to [PdCl(CH$_3$)(COD)], affording complex **1** in 67% isolated yield (Scheme 2). The $^{31}P\{^1H\}$ NMR spectrum of the product shows two singlets at δ_P = 36.2 and 35.8 in a 17 : 1 ratio ($CDCl_3$). The ^1H NMR spectrum also displays patterns for both imine and enamine moieties, indicating that the two species correspond to the two tautomeric forms **1a** and **1b**, respectively. The diagnostic doublets for the Pd-bound methyls for **1a** (0.47 ppm) and **1b** (0.61 ppm) have coupling constants of $^3J_{HP}$ = 3.4 and 3.6 Hz, respectively, which are consistent with a *cis* orientation of the phosphine and methyl for both tautomeric products.[18,20–22]

Single crystals were grown *via* slow vapour diffusion of pentane into a solution of **1** in a 9 : 1 mixture of toluene and

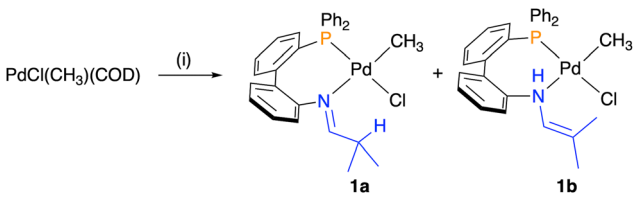

Scheme 2 Synthesis of the tautomeric mixture of palladium complexes **1a**/**1b**. Conditions: (i) 1.2 equiv. tautomeric mixture of ligand **H[L2]**, CH_2Cl_2, rt, 24 h. Product ratio **1a** : **1b** = 17 : 1.

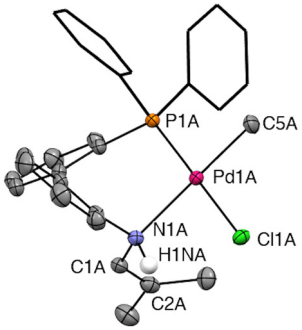

Fig. 3 Displacement ellipsoid plot of complex **1b**. Ellipsoids are given at 50% probability level, except the phenyl substituents of the phosphine donor that are depicted as wireframe for clarity. H atoms (except H1NA) were omitted for clarity. Selected bond distances (Å): N(1A)–C(1A) = 1.440(2), C(1A)–C(2A) = 1.332(3), Pd(1A)–N(1A) = 2.2483(15), Pd(1A)–P(1A) = 2.2085(8), Pd(1A)–C(5A) = 2.0351(18), Pd(1A)–Cl(1A) = 2.3871(9); selected angle (°): P(1A)–Pd(1A)–N(1A) = 95.18(5).

CH_2Cl_2 at −20 °C. X-ray diffraction revealed only the enamine tautomer **1b** (Fig. 3). The crystal structure contains two symmetry-independent molecules in the asymmetric unit, which are enantiomers and are designated as complex A and complex B. The structural parameters of only complex A will be discussed here since A and B have identical connectivity and very similar bond lengths and angles. The structure confirms a square planar geometry at the palladium centre, with very minimal distortion[23] according to the τ^4 value of 0.07. A *cis* orientation of the phosphine and methyl substituents is observed, which is consistent with the NMR spectroscopic data. The assignment of the structure as the enamine tautomer **1b** is supported by the bond lengths of N(1A)–C(1A) = 1.440(2) Å and C(1A)–C(2A) = 1.332(3) Å, which are characteristic of a C–N single bond and a C–C double bond, respectively. The P(1A)–Pd–N(1A) bite angle was determined to be 95.18(5)° (for B = 95.97(5)°), which is significantly wider than the angle of 78.48° found for the analogous complex with the monoaryl linked phosphine imine ligand **H[L1]**.[4] Therefore, **H[L2]** imparts less conformational strain on the metal centre and may allow for isolation of a Pd phosphine 1-azaallyl species in which the anionic ligand **L2** is coordinated in a κ^1-P;η^3-NCC mode.

Coordination of L2 with palladium

An initial strategy to access a phosphine 1-azaallyl complex involved deprotonation of the tautomeric mixture of the phosphine imine/enamine complexes **1a**/**1b**. However, these attempted deprotonation reactions produced complex reaction mixtures as evidenced by multiple signals in the $^{31}P\{^1H\}$ NMR spectrum, inconsistent with a well-defined product.

We therefore pursued an alternative route, in which the deprotonated ligand salt **K[L2]** was reacted with [$PdCl(CH_3)$(COD)] to afford an orange product **2** in a 70% yield (Scheme 3). The $^{31}P\{^1H\}$ NMR spectrum of isolated **2** has one singlet at δ_P = 25.7, consistent with phosphine coordination and formation of a single product. Several attempts were made

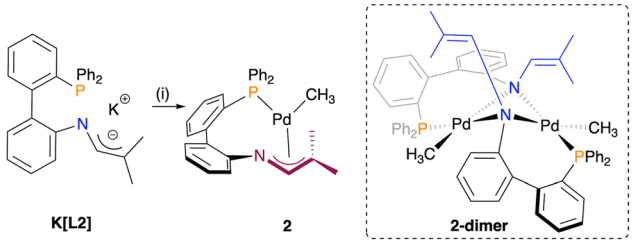

Scheme 3 Coordination of phosphine 1-azaallyl ligand **K[L2]** to palladium to form mononuclear **2**. Reaction conditions: (i) $PdCl(CH_3)$(COD), THF, rt, 10 min. COD = 1,5-cyclooctadiene. The characterized product **2** is depicted, along with an alternative possible structure **2-dimer**.

to afford X-ray quality crystals of **2**, but without success. However, the combination of NMR spectroscopy and X-ray absorption spectroscopy supported a κ^1-P;η^3-NCC coordination mode of **L2**, which corresponds to mononuclear **2**. This supporting evidence is as follows.

The chemical shifts of the carbon atoms of the 1-azaallyl fragment are highly diagnostic of metal coordination mode.[17] A combination of ^1H–^{13}C HSQC and ^1H–^{13}C HMBC allowed assignment of C^1 and C^2 of **2** at δ_C = 129.4 and 88.4, respectively (see Fig. 4a for atom numbering). By comparison, in complexes of **L1** where the 1-azaallyl group coordinates to the metal exclusively through nitrogen, the corresponding C^1 and C^2 resonances appear in the ranges 135–142 and 115–119 ppm, respectively.[17–19] The observed values for **2** fall well outside these ranges.

Among these signals, C^2 is particularly sensitive to the coordination environment. Its pronounced upfield shift in **2** is indicative of direct metal coordination at this carbon,[16,24] consistent with a κ^1-P;η^3-NCC binding mode. Furthermore, the

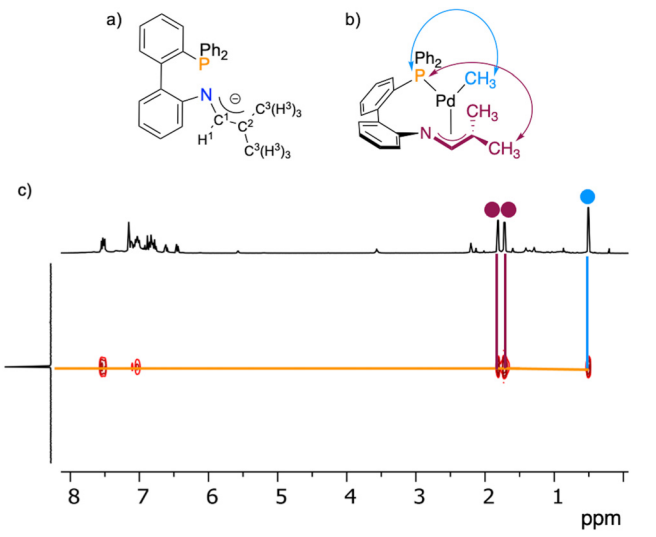

Fig. 4 (a) Structure of **L2** including relevant atom labels; (b) structure of **2** depicting observed 2D correlations; (c) ^1H–^{31}P HMBC NMR spectrum of **2** (600 MHz, C_6D_6). Assignment of labeled signals: ● = CH_3 substituents of the 1-azaallyl fragment; ● = CH_3 bound to Pd.

resonances for C^1, C^2, and C^3 are all observed as doublets due to coupling to phosphorus, whereas the corresponding signals in the previously reported dinuclear **B** are singlets.

Additional support for the κ^1-P;η^3-NCC mode was obtained from ^{1}H–^{31}P HMBC NMR spectroscopy (Fig. 4b and c). In this binding mode, protons $H^3/H^{3'}$ are within four bonds to the phosphine donor, which would be expected to give rise to an observable correlation. Such a correlation is indeed present for **2**. A conceivable alternative product of the reaction of **K[L2]** with [PdCl(CH$_3$)(COD)] is **2-dimer**, a complex analogous to **B**[18] (see Fig. 2). However, **2-dimer** would place $H^3/H^{3'}$ six bonds away from phosphorus, which would not give rise to a ^{1}H–^{31}P HMBC NMR correlation. Consistent with this expectation, dinuclear **B** shows no correlation between $H^3/H^{3'}$ and P in the ^{1}H–^{31}P HMBC NMR spectrum.[18] For the same reasons, a mononuclear THF solvate, [Pd(CH$_3$)(κ^2-PN-**L2**)(THF)], is also inconsistent with the observed spectroscopic data. Collectively, the NMR spectroscopic data supports assignment of **L2** as adopting a κ^1-P;η^3-NCC coordination mode, corresponding to assignment as the mononuclear structure **2**.

We pursued analysis of **2** by X-ray absorption spectroscopy (XAS) to further corroborate the assignment of **L2** coordination as κ^1-P;η^3-NCC, and to identify any unique properties of the palladium centre due to this coordination mode (Fig. 5). In addition to complex **2**, two other comparator Pd(II) complexes, **A** and **B** (see Fig. 2), coordinated by phosphine 1-azaallyl ligand **L1** were also studied. These compounds were selected since they exhibit distinct coordination modes of the 1-azaallyl group, in which **A** has κ^1-N and **B** has μ-N binding. The Pd L$_3$-edge XANES, the Pd K-edge EXAFS and the P K-edge XANES have been recorded and analyzed; the results are highlighted in Fig. 5, Fig. S52 and 53.

The Pd L$_3$-edge XANES shows sharp peaks for **2**, **A** and **B** around 3178 eV due to a $2p_{3/2} \rightarrow 4d$ transition (Fig. 5a). As expected, these peaks are found at a higher energy than those for the Pd(II) reference samples $PdCl_2$ and PdS, in which the transition promotes an electron into the conduction band of the solid-state materials. Compounds **A** and **B** have experimentally indistinguishable energy (3178.0 eV), while that for **2** is slightly lower (3177.9 eV). This suggests **2** is slightly more electrophilic, which may be a consequence of Pd coordination to the π-system of the 1-azaallyl fragment. Compound **B** exhibits an additional broad peak at ~3186 eV (marked by a green arrow), higher in relative energy to the $2p_{3/2} \rightarrow 4d$ transition. This energy range is typical for transitions due to multiple scattering from close proximity high-*Z* elements, which would be expected for the dinuclear Pd–N–Pd motif. The absence of a similar peak for **2** further discounts a bridging coordination mode for **L2** in **2** that would lead to a dinuclear structure.

The Pd K-edge XANES and EXAFS were acquired for **2**, **A**, **B** and references, and the Fourier transformed (FT) data was plotted in radial space (Fig. 5b). The Pd K-edge XANES is less sensitive than the Pd L$_3$-edge because the K edge has a much shorter core-hole lifetime than the L edge and has corresponding broader linewidths in XANES. However, the Pd K-edge EXAFS can still provide useful information on the local structure of Pd atoms. The dominant local bonding interaction is labelled for each sample. It should be noted that C and N have similar backscattering amplitude (*y* axis) and cannot be distinguished in the FT, as are P, S and Cl (the backscattering amplitude increases as the atomic number increases).

The known bonding environments for **A** and **B** both include phosphine, methyl and two N donors. They differ in that the N donors in **A** are Pd–N$_{(amido)}$ and Pd–N$_{(pyridine)}$, while in **B** they are two bridging amidos (*i.e.*, Pd–N$_{(amido)}$–Pd). Thus, the compounds give similar signatures, but the signal for **B** is observed at a slightly longer distance and higher amplitude. This could be due to the bridging nitrogens acting as lenses. As compared to **A** and **B**, the signal for **2** is notably at a shorter distance, has a lower amplitude, and has a shoulder as compared to **A** or **B**. A signal like that of **B** would be expected if **2** was also a bridging dinuclear complex, so the observed signal with dominant contribution from Pd–C/N further supports the assignment of **2** as a mononuclear compound supported by η^3-NCC coordination mode of the 1-azaallyl fragment.

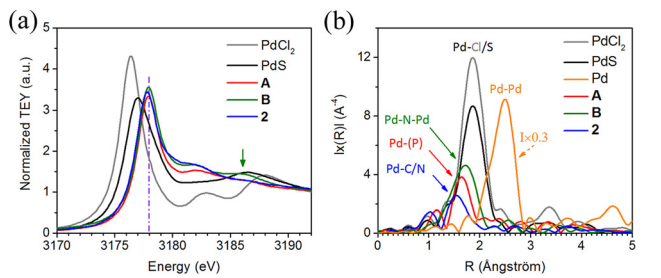

Fig. 5 XANES and EXAFS results for compounds **2**, **A**, **B** and reference compounds Pd metal, PdS and $PdCl_2$: (a) Pd L$_3$-edge XANES. The vertical dash-dotted line labels the maximum of the sharp peaks for **A** and **B**; (b) Fourier transform (FT) of the k^3-weighted Pd K-edge EXAFS in *R* space. The data in (b) shows the radial distance (before phase correction) of the neighbouring atoms surrounding Pd. The color-coded arrows show the corresponding dominant local bonding in compounds **2**, **A**, and **B**. The backscattering magnitude of Pd metal was reduced by 70% for comparison.

Substitution chemistry with complex 2

Our prior work with the Ru(II) phosphine 1-azaallyl complex **C** revealed that **L1** engages in a dynamic equilibrium between κ^2-PN and κ^1-P;η^3-NCC coordination modes (see Fig. 2).[19] This reversibility permitted facile coordination of Lewis basic donors to afford isolable coordinatively saturated complexes of the type Ru(Cp*)(κ^2-PN-**L1**)L (L = pyridine, PPh_3). Similarly, the dinuclear palladium complex **B** with κ^1-P;μ-N-(**L1**) readily reacts with pyridine to give the stable mononuclear adduct **A**.[18] Based on these prior studies, we hypothesized that Lewis basic donors would bind to **2**, and this would be accommodated by a change in **L2** coordination mode from κ^1-P;η^3-NCC to κ^2-P,N.

Complex **2** was treated with pyridine, and reactions were analyzed by ^{31}P{^{1}H} and ^{1}H NMR spectroscopy (Fig. 6, Fig. S2 and 3). The addition of 1 equivalent resulted in the broadening of the ^{31}P signal for **2** as well as many of the ^{1}H signals,

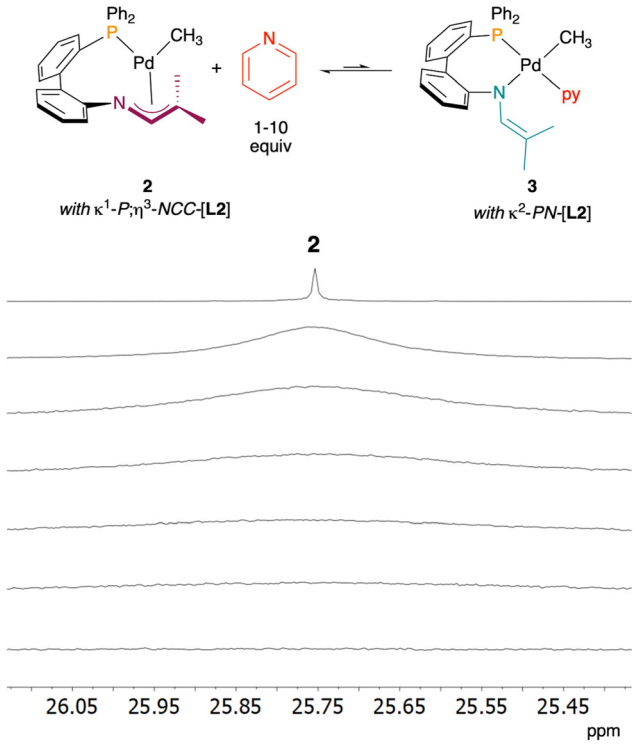

Fig. 6 (Top) Equilibrium reaction of **2** with pyridine to give adduct **3**, in which **L2** coordination modes are indicated. (Bottom) Expansion of the $^{31}P\{^1H\}$ NMR spectra (243 MHz, C_6D_6) stack plot of **2** with added pyridine equivalents of (top to bottom): 0, 1, 2, 3, 4, 5, 10.

indicative of equilibrium binding of pyridine. Increasing the pyridine equivalents up to 10 resulted in further broadening of both ^1H and ^{31}P signals. While signal broadening is consistent with chemical dynamics, the specific behaviour in this case is somewhat atypical. The broad signal is consistent with the fast exchange regime (*i.e.* relatively low-barrier exchange), for which the observed chemical shift should be a weighted average of the two species participating in the exchange.[25] In this case, we observe no notable difference in chemical shift between that of **2** and the broadened signal for 1 : 1 **2** and pyridine. We hypothesize that this is due to a very small K_{eq} value that strongly favours the reactants, and therefore the weighted average chemical shift is dominated by the value for **2**. This hypothesis is consistent with the observation that even 10 equiv. pyridine does not drive the equilibrium sufficiently to the proposed product **3**. Nevertheless, we considered that the disappearance of a ^{31}P signal could be due to formation of a paramagnetic product. An Evans analysis of a 1 : 1 mixture of **2** and pyridine did not reveal signal shifting due to paramagnetism (Fig. S4). Additionally, to confirm that **2** is an operative species in the observed equilibrium we designed an experiment to remove pyridine from the equilibrium mixture to regenerate **2**. A 1 : 1 mixture of **2** and pyridine was treated with excess $B(C_6F_5)_3$ to sequester pyridine in a Lewis acid base adduct (py → $B(C_6F_5)_3$). Sequestration was effective and **2** was regenerated, which confirmed that **2** is involved in the operative equilibrium (Fig. S6).

Evidence for the expected pyridine adduct **3** was obtained by variable temperature NMR spectroscopy. Dissolution of **2** in pyridine-d_5 at 25 °C resulted in a $^{31}P\{^1H\}$ spectrum with no observable signal (Fig. 7a, top spectrum). The ^1H NMR spectrum revealed a set of signals in which those of the 1-azaallyl fragment were noticeably broadened. Cooling the sample to −30 °C sharpened the ^1H signals, and a singlet emerged in the $^{31}P\{^1H\}$ NMR spectrum at 39.8 ppm (Fig. 7, Fig. S7 and 8). Low temperature ^1H and 2D NMR (^1H–^{31}P HMBC, ^1H–^1H COSY, ^1H–^{13}C HSQC, and ^1H–^{13}C HMBC) spectroscopy data were consistent with the formation of the pyridine adduct **3**. Notably, no correlation was observed between phosphorus and the protons of the 1-azaallyl methyl substituents $H^3/H^{3'}$ (Fig. 7b and c). Both C^1 and C^2 were shifted downfield relative to their location in **2** (**3**: 142 and 92 ppm, respectively). Taken together, this data indicates that **L2** is in the κ^2-PN coordination mode and that pyridine occupies a coordination site on the metal (*i.e.* **3**). The signal at δ_P = 39, assigned to **3**, was also observed below 0 °C for a 1 : 4 mixture of **2** and pyridine in toluene-d_8 (Fig. S13). To confirm that the low temperature product is the pyridine adduct **3**, and not **2-dimer**, VT NMR spectra of **2** in toluene-d_8 were collected. No signal at 39 ppm emerged in the temperature range of 25 to −80 °C (Fig. S15 and S16).

The fact that pyridine adduct **3** is only directly observed at low temperatures and in the presence of excess pyridine is remarkable given that isolation of the related pyridine adduct [$PdCH_3$(BINAP)(py)]OTf is possible (BINAP = 2,2′-bis(diphenylphosphino)-1,1′-binaphthyl).[26] The κ^2 bite angles of BINAP and **L2** are close (BINAP = 93°,[27] H[**L2**] = 95°), so similar stability of the pyridine adducts could be expected. The key difference between BINAP and **L2** is the capacity of the latter to access the κ^1-P;η^3-NCC mode, which is evidently much more

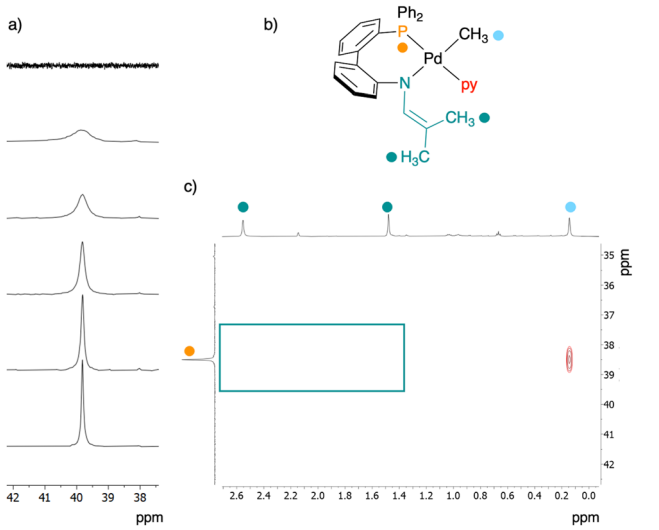

Fig. 7 (a) Expansion of the $^{31}P\{^1H\}$ NMR spectra (243 MHz) of **2** dissolved in pyridine-d_5 at temperatures of (top to bottom): 25, 10, 0, −10, −20, and −30 °C, (b) labelling scheme for relevant signals from compound **3**, (c) expansion of the ^1H–^{31}P HMBC (600 MHz) of **2** dissolved in pyridine-d_5 collected at −30 °C.

stable than the bidentate mode, and this induces pyridine dissociation from **3**.

The experimental studies of the reaction of **2** with pyridine as reported above suggest that the energetic landscape of the various **L2** binding modes is relatively shallow, a feature that is often advantageous in catalysis. To support this interpretation, we used density-functional theory methods to examine the reaction **2** + **py** ⇌ **3** (Fig. 6) in benzene solution. In principle, this reaction can proceed by either (a) an associative mechanism involving a transition state (**TS**) or (b) a dissociative mechanism in which the κ^1-P;η^3-NCC coordination mode of **2** shifts to κ^2-PN to give a three-coordinate intermediate (**2-open**), followed by addition of pyridine. Formation of **2-dimer** is also a possible side process. To assess these pathways, we computed zero-point-energy-corrected electronic energies (ΔE_0) and Gibbs free energies (ΔG) of the species involved.

The calculations were carried out using the PBE1PBE hybrid functional in combination with the def2-TZVP basis set, Grimme's D4 empirical dispersion correction, and the SMD implicit solvation model, as implemented in the Gaussian Development Version.[28] The chosen level of theory provides a well-established balance of accuracy and efficiency for transition-metal complexes of similar complexity. The results are summarized in Table 1. The reported values are not claimed to be highly accurate, but they lead to the same qualitative conclusions as the PBEh-3c [29] and B97h-3c [30] composite methods (Tables S2 and S3), as well as PBE1PBE calculations with a smaller basis set (Table S4).

According to Table 1, complex **3** is more stable than **2** + **py** at low temperatures, while **2-dimer** is always more stable than both **3** and **2** + **py**. Thermodynamics alone would therefore suggest that dimer formation should be preferred. However, the kinetic landscape is markedly different.

An explicit **TS** was located for the **2** + **py** → **3** pathway (Fig. S54), and it lies only 0.2 kJ mol^{-1} above the reactants on the potential energy surface (with zero-point-energy corrections). Therefore, the formation of **3** would have practically no barrier at 0 K; even at −30 °C, the Gibbs energy of the **TS** is only $\Delta G^{\ddagger}_{243}$ = +36.9 kJ mol^{-1} relative to the reactants. Because of the limitations of the harmonic oscillator/ideal-gas approximation, thermal corrections in this system are almost certainly overestimated, which means than the true $\Delta G^{\ddagger}_{243}$ could be even lower. This relatively low barrier is consistent with facile formation of **3** at reduced temperature.

On the other hand, even though the activation barrier for the dimer formation was not computed, it necessarily exceeds 43 kJ mol^{-1} relative to **2** (assuming the dimerization proceeds through **2-open**), and is likely substantially higher because of entropic penalties. The higher activation barrier for **2-dimer** supports the observation that the dimerization pathway is not observed.

As for the dissociative path from **2** to **3**, the putative intermediate **2-open** lies consistently higher than **2**, with ΔE_0 = +45.5 kJ mol^{-1} and ΔG_{243} = +43.0 kJ mol^{-1}. Since we did not attempt to locate the transition state between **2** and **2-open**, the possibility of the competing dissociative substitution pathway from **2** to **3** cannot be excluded, but this does not affect the above conclusion that **2-dimer** is kinetically disfavoured.

Taken together, the data of Tables 1 and S2–S4 provide a consistent mechanistic explanation: **3** is the kinetically accessible product at low temperature, whereas dimer formation is apparently rendered negligible by unfavourable entropic factors.

The relatively small Gibbs energy difference between **2** + **py** and **3** at 243–298 K shows that **L2** binding can readily change to accommodate different numbers of exogenous ligands on the metal. The preference for **L2** binding *via* the κ^1-P;η^3-NCC mode promotes dissociation of the Lewis base pyridine. Thus, the dynamic coordination chemistry of **L2** offers a low-energy pathway for substitution reactions at Pd.

Table 1 Calculated relative energies (in kJ mol^{-1}) of various structures involving the **L2** ligand[a]

Structure	ΔE_0	ΔG_{243}	ΔG_{298}
2 + **py**	0.0	0.0	0.0
TS	0.2	36.9	46.2
3	−40.5	0.0	9.0
2-open + **py**	45.5	43.0	42.2
2-dimer[b]	−49.9	−21.7	−15.6

[a] Method: PBE1PBE/def2-SVP EmpiricalDispersion = GD4 SCRF (SMD, solvent = benzene). All data are referenced to the ideal-gas standard state of 1 atm for each species, whether solvated or not. [b] Relative to **2** per mole of monomer

Conclusions

A new ligand **L2** with phosphine and 1-azaallyl donor groups was prepared that has a wider κ^2-PN bite angle than a previous ligand derivative (*i.e.*, **L1**). This characteristic permitted access to the κ^1-P;η^3-NCC coordination mode within a Pd(II)-methyl complex, **2**. The mode was confirmed through characterization of **2** by NMR and X-ray absorption spectroscopies. The Pd L_3-edge XANES measurements revealed that the κ^1-P;η^3-NCC coordination mode may lead to enhanced electrophilicity of Pd in **2**, which is desirable for Lewis base coordination. Attempts to prepare a Lewis acid–base adduct of **2**, in which **L2** would adopt a κ^2-PN mode to accommodate the new ligand, resulted in dynamic mixtures. The adduct **3** was observed, but only in the presence of an excess of pyridine and at low temperatures. Electronic structure calculations confirmed the energetic proximity of **2** and the pyridine adduct **3**, which facilitates the observed reversible attachment of the Lewis base ligand.

The capacity of the ligand to facilitate reactions with shallow energic pathways is a generally desirable feature of catalysts. For example, **2** may readily permit facile substrate coordination (*i.e.*, Lewis base coordination) and product dissociation (*i.e.*, Lewis base dissociation), without catalyst inhi-

bition. We are currently exploring applications of **2** and related compounds in catalysis.

Author contributions

The manuscript was written through contributions of all authors.

Conflicts of interest

There are no conflicts to declare.

Data availability

Supplementary information (SI): NMR spectroscopy, IR spectroscopy, UV-vis spectroscopy, mass spectrometry, X-ray absorption spectroscopy, and computational (optimized *XYZ* coordinates) data. See DOI: https://doi.org/10.1039/d5dt02402a.

CCDC 2487843 (**1b**) contains the supplementary crystallographic data for this paper.[31]

Acknowledgements

The authors acknowledge the support of the Natural Sciences and Engineering Research Council (NSERC) of Canada Discovery Grants Program (V. N. S., T. K. S., and J. M. B.). Part of the research described in this paper was performed at the Canadian Light Source, a national research facility of the University of Saskatchewan, which is supported by the Canada Foundation for Innovation (CFI), the Natural Sciences and Engineering Research Council (NSERC), the National Research Council (NRC), the Canadian Institutes of Health Research (CIHR), the Government of Saskatchewan, and the University of Saskatchewan.

References

1 J. F. Hartwig, *Organotransition Metal Chemistry: From Bonding to Catalysis*, University Science Books Sausalito, CA, 2010.
2 R. H. Crabtree, *The Organometallic Chemistry of the Transition Metals*, Wiley-Interscience, Hoboken, N.J, 2005.
3 R. B. Jordan, *Reaction Mechanisms of Inorganic and Organometallic Systems*, Oxford University Press, New York, 3 edn, 2007.
4 J. M. Blacquiere, *ACS Catal.*, 2021, **11**, 5416–5437.
5 P. Braunstein and F. Naud, *Angew. Chem., Int. Ed.*, 2001, **40**, 680–699.
6 C. S. Slone, D. A. Weinberger and C. A. Mirkin, in *Prog. Inorg. Chem*, ed. K. D. Karlin, John Wiley& Sons, Inc., 1999, vol. 48, pp. 233–350.
7 M. Bassetti, *Eur. J. Inorg. Chem.*, 2006, **2006**, 4473–4482.
8 G. M. Adams and A. S. Weller, *Coord. Chem. Rev.*, 2018, **355**, 150–172.
9 D. G. A. Verhoeven and M.-E. Moret, *Dalton Trans.*, 2016, **45**, 15762–15778.
10 A. Beaufils, P. Melle, N. Lentz and M. Albrecht, *Inorg. Chem.*, 2024, **63**, 2072–2081.
11 K. D. Sipps, W. A. Gibbs, E. R. Sayfutyarova and J. L. Kuo, *ACS Catal.*, 2024, **14**, 18045–18054.
12 B. M. Trost and M. C. Ryan, *Angew. Chem., Int. Ed.*, 2017, **56**, 2862–2879.
13 M. J. Calhorda, C. C. Romão and L. F. Veiros, *Chem. – Eur. J.*, 2002, **8**, 868–875.
14 D. Zargarian, *Coord. Chem. Rev.*, 2002, **233–234**, 157–176.
15 C. F. Caro, M. F. Lappert and P. G. Merle, *Coord. Chem. Rev.*, 2001, **219–221**, 605–663.
16 A. G. Avent, P. B. Hitchcock, M. F. Lappert, R. Sablong and J. R. Severn, *Organometallics*, 2004, **23**, 2591–2600.
17 J. M. Stubbs, K. F. Firth, B. J. Bridge, K. J. Berger, R. J. Hazlehurst, P. D. Boyle and J. M. Blacquiere, *Dalton Trans.*, 2017, **46**, 647–650.
18 K. M. K. Jackman, B. J. Bridge, E. R. Sauvé, C. N. Rowley, C. H. M. Zheng, J. M. Stubbs, P. D. Boyle and J. M. Blacquiere, *Organometallics*, 2019, **38**, 1677–1681.
19 M. B. Kindervater, V. N. Staroverov, K. M. K. Jackman, A. A. Fogh, L. S. G. Kelley, L. Lim, S. A. Sirohey, P. D. Boyle and J. M. Blacquiere, *Dalton Trans.*, 2023, **52**, 10744–10750.
20 X. Zhou, K.-C. Lau, B. J. Petro and R. F. Jordan, *Organometallics*, 2014, **33**, 7209–7214.
21 N. D. Contrella, J. R. Sampson and R. F. Jordan, *Organometallics*, 2014, **33**, 3546–3555.
22 T. Kochi, S. Noda, K. Yoshimura and K. Nozaki, *J. Am. Chem. Soc.*, 2007, **129**, 8948–8949.
23 L. Yang, D. R. Powell and R. P. Houser, *Dalton Trans.*, 2007, 955–964.
24 P. B. Hitchcock, M. F. Lappert and M. Layh, *Z. Anorg. Allg. Chem.*, 2000, **626**, 1081–1086.
25 N. E. Jacobsen, in *NMR Spectroscopy Explained*, ed. N. E. Jacobsen, John Wiley & Sons, Inc., 2007, pp. 408–488, DOI: 10.1002/9780470173350.ch10.
26 A. M. Johns, J. W. Tye and J. F. Hartwig, *J. Am. Chem. Soc.*, 2006, **128**, 16010–16011.
27 M.-N. Birkholz, Z. Freixa and P. W. N. M. van Leeuwen, *Chem. Soc. Rev.*, 2009, **38**, 1099–1118.
28 M. J. Frisch, G. W. Trucks, G. Scalmani, J. R. Cheeseman, X. Li, J. Bloino, B. G. Janesko, A. Marenich, J. Zheng, F. Lipparini, A. Jenkins, A. Liu, H. Liu, H. B. Schlegel, G. E. Scuseria, M. A. Robb, V. Barone, G. A. Petersson, H. Nakatsuji, B. Mennucci, C. Adamo, N. Rega, M. Caricato, H. P. Hratchian, J. V. Ortiz, F. Pawlowski, A. F. Izmaylov, H. Hu, C. Liao, J. L. Sonnenberg, D. Williams-Young, F. Ding, R. Gomperts, F. Egidi, J. Goings, B. Peng, A. Petrone, T. Henderson, D. Ranasinghe, V. G. Zakrzewski, J. Gao, G. Zheng, W. Liang, M. Hada, M. Ehara, K. Toyota, R. Fukuda, J. Hasegawa, M. Ishida, T. Nakajima, Y. Honda, O. Kitao, H. Nakai, T. Vreven, K. Throssell, J. A. Montgomery Jr., J. E. Peralta, F. Ogliaro, M. J. Bearpark, J. J. Heyd,

E. N. Brothers, K. N. Kudin, V. N. Staroverov, T. A. Keith, R. Kobayashi, J. Normand, K. Raghavachari, A. P. Rendell, J. C. Burant, S. S. Iyengar, M. Cossi, J. M. Millam, M. Klene, R. Cammi, R. L. Martin, O. Farkas, J. B. Foresman and D. J. Fox, *Gaussian Development Version, Revision J.28*, Gaussian, Inc., Wallingford, CT, 2023.

29 S. Grimme, J. G. Brandenburg, C. Bannwarth and A. Hansen, *J. Chem. Phys.*, 2015, **143**, 054107.

30 J. G. Brandenburg, C. Bannwarth, A. Hansen and S. Grimme, *J. Chem. Phys.*, 2018, **148**, 064104.

31 CCDC 2487843: Experimental Crystal Structure Determination, 2026, DOI: 10.5517/ccdc.csd.cc2pht01.